Electronic Supplementary Material (ESI) for Lab on a Chip.

Versatile acoustic manipulation of micro-object using mode-switchable oscillating bubbles: transportation, trapping, rotation, and revolution

Wei Zhang,[‡,1] *Bin Song,*[‡,1] *Xue Bai,*[1] *Lina Jia,*[1] *Li Song,*[1] *Jingli Guo,*[1] *Lin Feng**[1,2]

[1] School of Mechanical Engineering & Automation, Beihang University, Beijing 100191, China

[2] Beijing Advanced Innovation Center for Biomedical Engineering, Beijing 100083, China

*Corresponding author: linfeng@buaa.edu.cn

The PDF file includes:

Text:

Figures:

Table:

Other Supplementary Material for this manuscript includes the following:

Video S1 (.mp4 format). Generation of bottom bubble array in the microchannel.

Video S2 (.mp4 format). Continuable switching between several bubble streaming patterns.

Video S3 (.mp4 format). Flexible manipulation-switching induced by bubble streaming.

Video S4 (.mp4 format). Unidirectional transportation of micro-objects

Video S5 (.mp4 format). Long-distance transportation of a single *E. gracili*.

Video S6 (.mp4 format). Rotational modes of DU145 cells.

Video S7 (.mp4 format). Rotational manipulation of particles and *E. gracilis*.

Video S8 (.mp4 format). Circular revolution of micro-objects.

Video S9 (.mp4 format). 3D cell reconstruction based on the out-of-plane rotation.

Text:

Supplementary Note S1: Theoretical influence of bubble interaction on the acoustic streaming

Theoretically, the interaction of oscillating bubbles is associated with secondary radiation force. In order to simplify calculating, the secondary radiation force F_{sr} of two same-sized bubbles is given as:[1,2]

$$F_{sr} = \frac{2\pi|p_0|^2 a^2}{\rho_1 \omega^2 L^2 |D_0|^2}\left(\left(\frac{\omega_0^2}{\omega^2} - 1 + \frac{a}{L}\right)^2 + \delta^2\right), \quad (1)$$

$$D_0 = \left(\frac{\omega_0^2}{\omega^2} - 1 - i\delta\right)^2 - \frac{a^2}{L^2}. \quad (2)$$

where a, ω, ω_0, δ are the radius, driving frequency, resonant frequency and dissipation factor of the trapped bubbles, respectively. L is the distance between two identical microbubbles. According to the expression of F_{sr}, interaction of neighboring bubbles mainly depends on the configuration parameters of microbubbles and could be evaluated by the ratio of bubble radius (a) to the distance (L) and the transition ratio is around 0.02. Therefore, for the design of our work, the interaction of neighboring bubbles exists and would influences the leading microstreaming around bubbles as shown in our experiments.

The leading streaming field around several bubbles could be regarded as the superposition of each field induced by the individual bubble. Therefore, the leading streamfunction in each mode could be written as:[3,4]

$$\varphi = \varphi_1 + \varphi_2. \quad (3)$$

where φ_i (i=1, 2) denotes the streamfunction of a single bubble. Therefore, eqn (3) reflects that the key tendency of the streaming pattern was not changed by the interaction of bubbles, while

there exist deforming parts and strengthening of streaming velocity.

Supplementary Note S2: Force principles in the bubble-induced microstreaming flow

The Reynolds number of the microbubble-induced microstreaming can be estimated as follows:[5]

$$Re = \varepsilon^2 (\frac{\omega}{\eta a^2})^{1/2} \approx 0.02, \quad (4)$$

where $\varepsilon = 2.5\ \mu m$ is the oscillation amplitude; $\omega = 2\pi f$ is the angular driving frequency, $a = 50\ \mu m$ is the radius of the bottom trapped bubble, and $\eta = 10^{-6}\ m^2 s^{-1}$ is the kinematic viscosity of the surrounding fluid. A low Reynolds number allows us to instantaneously control the appearance and disappearance of acoustic microstreaming by turning on and off the power.

When micro-objects, like microbeads or cells, are loaded near an oscillating microbubble in an acoustic field, two principle acoustic forces are scattered: the microstreaming-induced viscous drag force, and the acoustic radiation force generated by the oscillating bubble. The viscous drag force (induced by microstreaming) directs the micro-objects of different sizes or shapes to move along the streamline in the fluid. The drag force on a bio-sample can be estimated according to the principle of a round sphere surrounded by the flow at a low Reynolds number, and it is defined by the following formula:[6]

$$F_d = 6\pi\eta R_c\, U, \quad (5)$$

where U is the relative velocity; $R_c = 10\ \mu m$ is the radius of the micro-object. The maximum drag force was calculated at 0.27 nN. The secondary acoustic radiation force, which is called the Bjerknes force, can be expressed as:[7]

$$F_r = 4\pi \frac{\rho_f - \rho_p\ R_b^4 R_f^3}{\rho_f + 2\rho_p\ \ d^5} \omega^2 \varepsilon^2 \quad (6)$$

.

where d is the distance between the centers of the microbubble and the micro-object, and ρ_f and ρ_p are the densities of the surrounding medium and the micro-object, respectively. The maximum Bjerknes force was calculated at 0.02 pN, which was much smaller than the previously calculated maximum drag force, indicating that the manipulated cells were mainly subjected to the drag force in our experiments.

In addition, according to eqn (6), the Bjerknes force can be either attractive or repulsive. The former happens when the density of the surrounding medium is lower than that of the micro-object, the bubble; on the contrary, this force can be repulsive because of the surrounding medium having a higher density. In accordance with the theoretical results, DU145 cells were attracted to the oscillating bubble in the experiments.

Supplementary Note S3: Heat measurement

Heart generation induced from acoustic energy has potential impacts on cell viability during acoustic manipulation. Since the piezoelectric transducer is the main heat source in the system due to its electromechanical losses,[8] the temperature change of the transducer surface is worth reference for the heat generation of the system. Therefore, a thermal imaging camera (FLIR-E6390, FLIR, Sweden) was utilized to measure the temperature of our acoustofluidic device. Measurements were conducted by activating the transducer at 20 Vpp and at 4.4 kHz for 20 minutes (higher power than the ones in the manipulation experiments). As shown in Fig. S5, the initial surface temperature of the transducer was 22.1 °C, and a final temperature of 24.3 °C was monitored after 20 min operation. The rises of temperature at the driving frequency were less than 3 °C and the final temperature is lower than human body temperature. The results suggest that the heat generated from the transducer has little effect on cell damage in the work.

Figures:

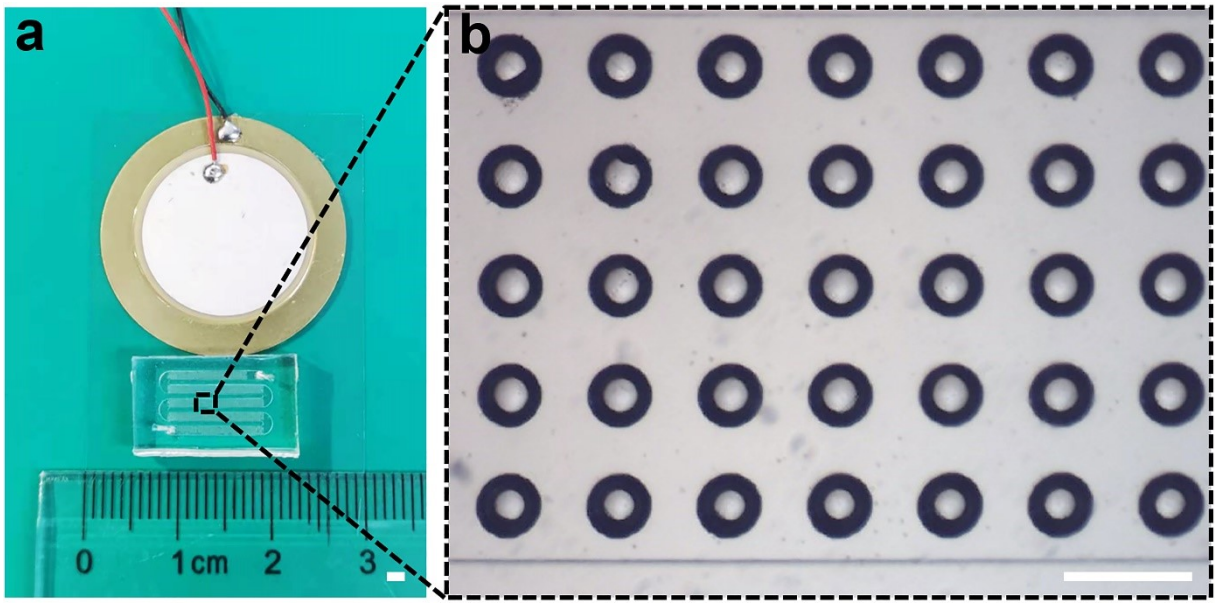

Fig. S1 Images of the bubble-based acoustofluidic device. (a) Photograph of an assembled acoustofluidic device with bottom bubble arrays. (b) Optical image showing bottom bubbles trapped over the microcavities in the microchannel. The generated bubbles among the two-dimensional arrays remain generally uniform in size and further execute the same oscillation mode in the static microfluid. Scale bar: 200 μm.

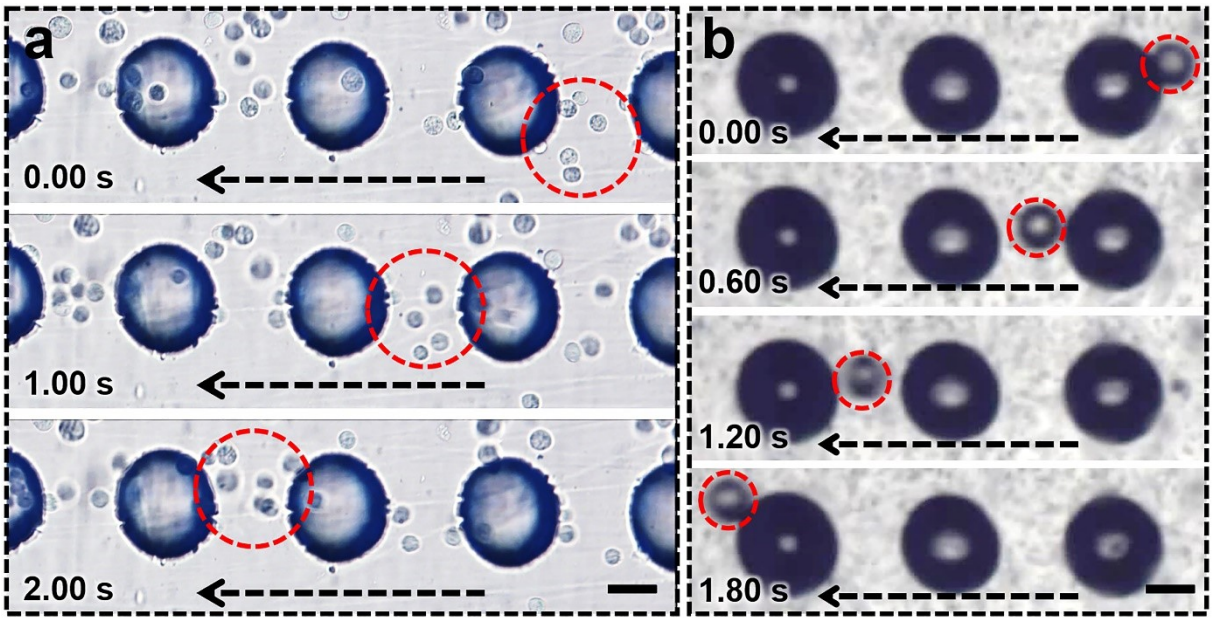

Fig. S2 Sequences visualizing the unidirectional transportation of (a) numerous DU145c and (b) single 50 µm particle. The excitation frequency and voltage are applied at 4.0 kHz and 5 Vpp, respectively. Scale bar: 50 µm.

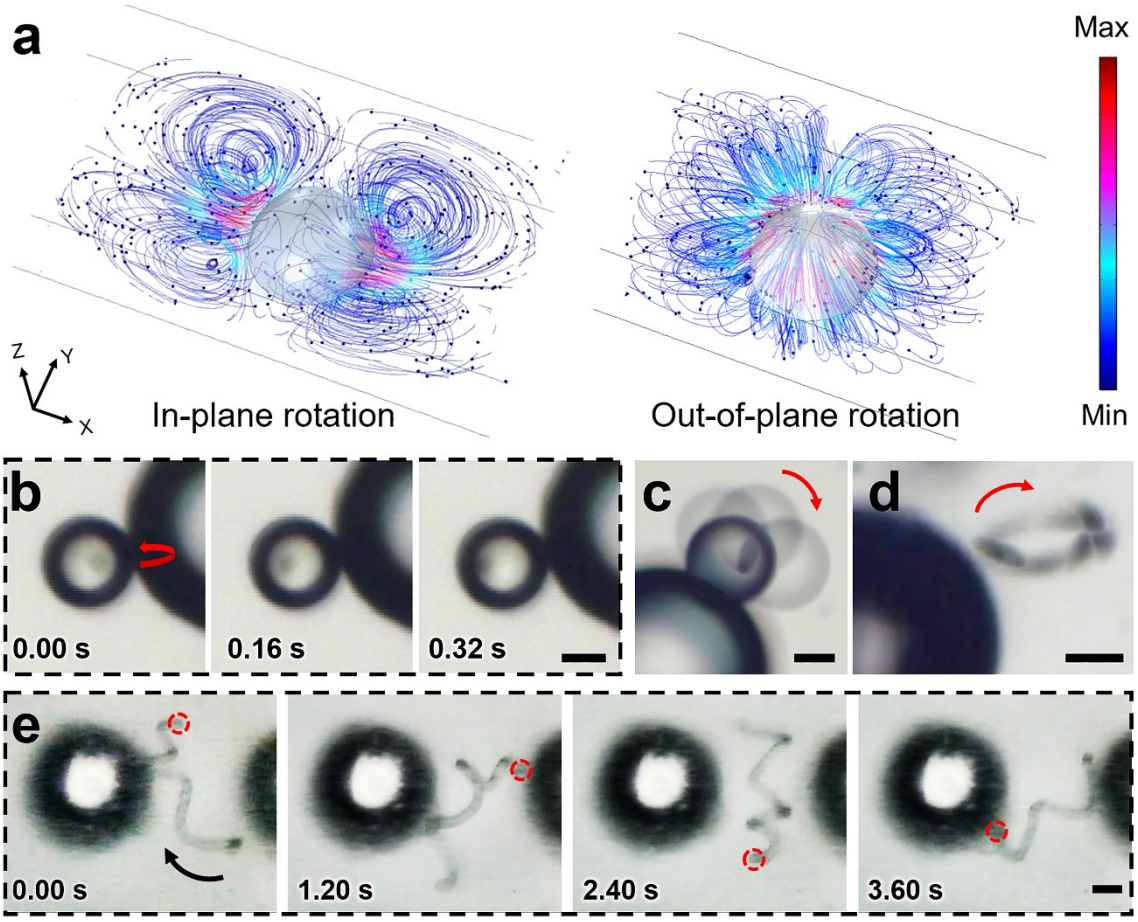

Fig. S3 Numerical illustrations and rotational manipulation of micro-objects. (a) 3D simulation of bubble streaming pattern in the in-plane and out-of-plane rotational mode. (b) Out-of-plane rotation of single 50 µm particle. (c)–(d) Rotation of an unfixed 50 µm particle and *E. gracili* showing that uncaught samples flow along rotational vortices. (e) In-plane rotation of *Spirulina.* Scale bar: 25 µm.

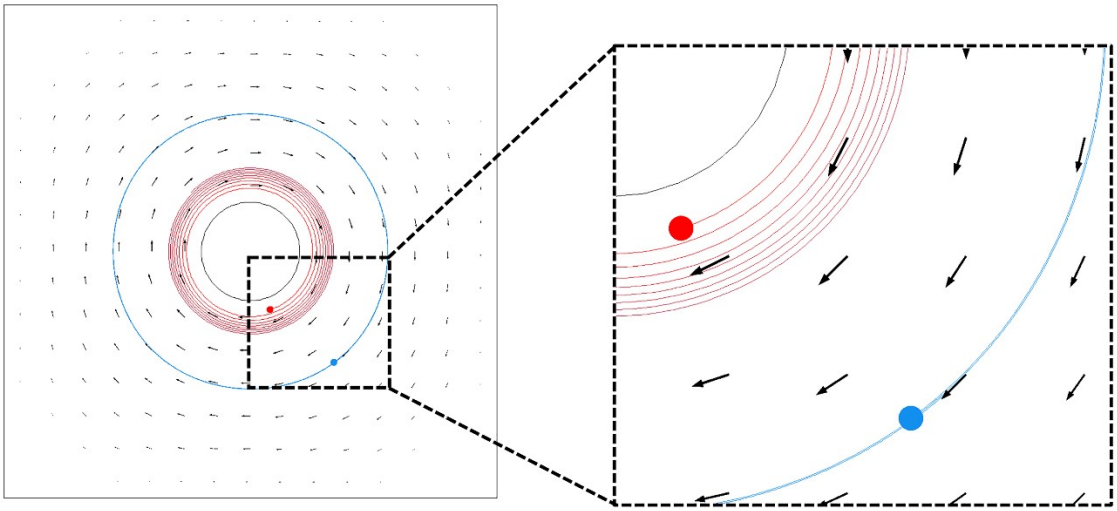

Fig. S4 Simulated results of particle trajectory in the circular revolution mode. Particles in two different positions was attracted on different levels during their revolving due to acoustic radiation force.

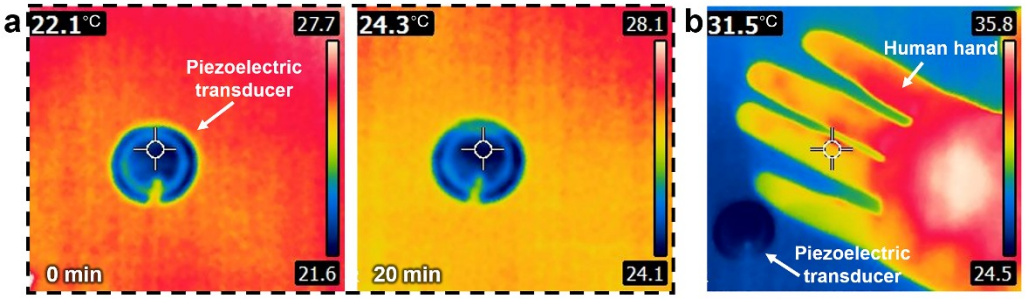

Fig. S5 Temperature measurement of the transducer surface by thermal imaging camera. (a) Temperature change in 20-min acoustic actuation. (b) Temperature comparison between a human hand and the transducer during acoustic operation.

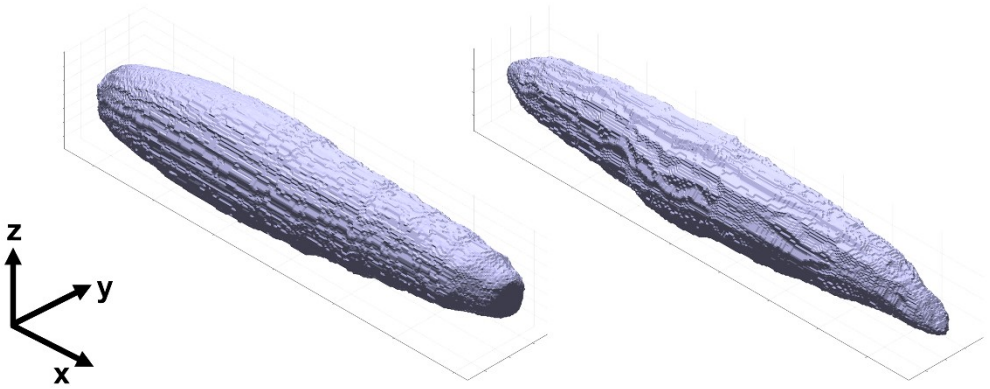

Fig. S6 Reconstruction model of rotated *E. gracilis*.

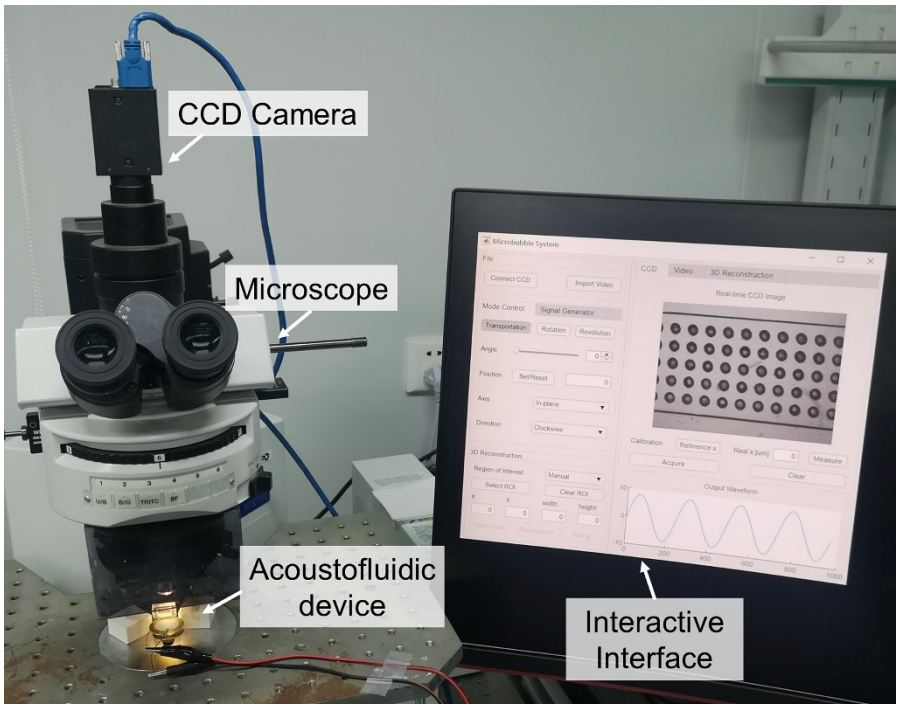

Fig. S7 Snapshot of the integrated driving system.

Table S1 Parameters of the experimental micro-objects

Experimental Sample	**Microbead**	**Cell**	**Organism**	
		Cancer cell	*E. gracili*	*Spirulina*
Diameter (μm)	1 3 20 50	20-25	50-100	~200
Shape	Sphere	Sphere	Long fusiform	Helical

Supplementary References:

[1] E. Zabolotskaya, Sov. Phys. *Acoust.-USSR*, 1984, **30**, 365-368.

[2] Y. Zhang, Y. Zhang and S. Li, *Ultrason. Sonochem.*, 2016, **29**, 129-145.

[3] A. A. Doinikov and A. Bouakaz, *J. Fluid Mech.*, 2016, **796**, 318-339.

[4] A. A. Doinikov, T. Combriat, P. Thibault and P. Marmottant, *Phys. Rev. E*, 2016, **94**, 033109.

[5] P. Marmottant and S. Hilgenfeldt, *Nature,* 2003, **423**, 153-156.

[6] P. Rogers and A. Neild, *Lab Chip,* 2011, **11**, 3710-3715.

[7] Y. Chen, Z. Fang, B. Merritt, D. Strack, J. Xu and S. Lee, *Lab Chip,* 2016, **16**, 3024-3032.

[8] M. Wiklund, *Lab Chip*, 2012, **12**, 2018-2028.